Mon. Not. R. Astron. Soc. **000**, 1–15 (2007) Printed 12 January 2011 (MN LATEX style file v2.2)

The Galaxy Population of Abell 1367: The Stellar Mass-Metallicity Relation

M. Mouhcine[1], W. Kriwattanawong[1,2], P. A. James[1]
[1] *Astrophysics Research Institute, Liverpool John Moores University, Twelve Quays House, Egerton Wharf, Birkenhead, CH41 1LD, UK*
[2] *Department of Physics and Materials Science, Faculty of Science, Chiang Mai University*

Accepted ?. Received ?; in original form ?

ABSTRACT

Using wide baseline broad-band photometry, we analyse the stellar population properties of a sample of 72 galaxies, spanning a wide range of stellar masses and morphological types, in the nearby spiral-rich and dynamically young galaxy cluster Abell 1367. The sample galaxies are distributed from the cluster centre out to approximately half the cluster Abell radius. The optical/near-infrared colours are compared with simple stellar population synthesis models from which the luminosity-weighted stellar population ages and metallicities are determined. The locus of the colours of elliptical galaxies traces a sequence of varying metallicity at a narrow range of luminosity-weighted stellar ages. Lenticular galaxies in the red sequence, however, exhibit a substantial spread of luminosity-weighted stellar metallicities and ages. For red sequence lenticular galaxies and blue cloud galaxies, low mass galaxies tend to be on average dominated by stellar populations of younger luminosity-weighted ages. Sample galaxies exhibit a strong correlation between integrated stellar mass and luminosity-weighted stellar metallicity. Galaxies with signs of morphological disturbance and ongoing star formation activity, tend to be underabundant with respect to passive galaxies in the red sequence of comparable stellar masses. We argue that this could be due to tidally-driven gas flows toward the star-forming regions, carrying less enriched gas and diluting the pre-existing gas to produce younger stellar populations with lower metallicities than would be obtained prior to the interaction. Finally, we find no statistically significant evidence for changes in the luminosity-weighted ages and metallicities for either red sequence or blue cloud galaxies, at fixed stellar mass, with location within the cluster.

Key words: galaxies: formation – galaxies: stellar content

1 INTRODUCTION

Clusters of galaxies are unique laboratories for studying the impact of the environment on galaxy properties. A large body of observational evidence has been collected over decades testifying that the properties and evolution of galaxies are strongly linked to their environment. The populations of galaxies in clusters tend to have spheroid-dominated morphologies (e.g. Dressler 1980; Dressler et al. 1997) with little or no ongoing star formation (e.g. Butcher & Oemler 1984; Lewis et al. 2002), in striking contrast with the properties of the dominant galaxy population in the field. What is unknown, however, is which dominant mechanisms cause this dichotomy, and in what kind of environments they mainly operate.

The hierarchical formation scenario predicts that galaxy clusters are formed by accretion of building blocks of smaller mass at the nodes of large-scale filaments (West et al. 1991; Katz & White 1993). The spiral-rich cluster Abell 1367 ($z \sim 0.0216$) lies at the intersection of two filaments in the Great Wall. The complex dynamical state of the cluster points towards the presence of multiple substructures falling into the core (e.g. Cortese et al. 2004) suggesting a comparatively recent formation of the cluster. These substructures contain a higher fraction of star forming galaxies than the cluster core, as expected during a merger event. This galaxy cluster is a rather unusual example of local, rich, dynamically young clusters since, in addition to massive evolved substructures, it is also experiencing the merging of a compact group directly falling into its core as revealed by deep

[1] We dedicate this work to the memory of our friend and colleague C. Moss who died suddenly recently.

narrow-band imaging, representing the region with the highest density of star forming systems ever observed in the local Universe (Sakai et al. 2002; Cortese et al. 2004). X-ray observations of Abell 1367 show multiple clumps, extended gas features and a strong localised shock in the intra-cluster medium (Grebenev et al. 1995; Donnelly et al. 1998), that could be associated with a merging component in the process of penetrating the cluster. More recent X-ray data indicate the presence of cool gas streaming into the cluster core (e.g. Sun & Murray 2002), supporting a multiple merger scenario. Optical and radio observations also suggest that this cluster is currently experiencing group infall into its centre (Gavazzi et al. 2001, 2003). The cluster has a high fraction of blue star-forming galaxies, which are more likely to appear disturbed and show evidence of tidal interaction driven star formation than similar galaxies in the field (Moss et al. 1998; Moss & Whittle 2000, 2005). In addition, galaxies exhibit the effects of ram-pressure of the inter-galactic medium (IGM; Gavazzi et al. 2001).

The ages and the chemical properties of the stellar contents of galaxies are direct tracers of their star formation and chemical enrichment histories. Determining the properties of the current stellar population in galaxies allows the possibility of constraining the formation histories. Clues to the properties of the stellar content, i.e., ages, metallicities, and abundance ratios, of unresolved objects may be inferred from their integrated energy distribution. The problem is complicated, however, as the energy distributions of integrated stellar populations respond to variations of different parameters in degenerate ways. The most known of those is the so-called age-metallicity degeneracy (e.g. Faber 1973; Rose 1985; Worthey 1994), whereby optical broad-band colours and most absorption line strengths respond similarly to changes in age and metallicity. Major improvement was brought by the introduction of the Lick/IDS system (Burstein et al. 1984) and its extension to high-order Balmer lines (Worthey & Ottoviani 1997), which popularized the measurement of absorption line strengths in the spectra of galaxies. The development of models to predict the strengths of absorption indices as a function of stellar population parameters (e.g. Worthey 1994; Bressan et al. 1994; Vazdekis 1999; Thomas et al. 2003; Schiavon 2007) has shown that metallic lines and Balmer lines show different sensitivities to ages and metallicities, thus allowing the age-metallicity degeneracy to be broken.

A complementary approach to derive constraints on stellar population ages and metallicities is the use of optical/near-infrared colours (e.g. James et al. 2006; Lee et al. 2007). A number of observational studies highlight the potential of the combination of optical and near-infrared (hereafter near-IR) integrated colours for breaking the age-metallicity degeneracy for both globular clusters (e.g. Puzia et al. 2002; Hempel & Kissler-Pating 2004), and stellar systems with complex star formation histories (e.g. Peletier et al. 1990; Peletier & Balcells 1996; Smail et al. 2001; MacArthur et al. 2004). James et al. (2006) have used the suite of models used in the present paper to investigate the extent to which the stellar population parameters derived from broad-band optical/near-IR agree with other constraints derived independently. They found that the colours of the Large Magellanic Cloud and M31 globular clusters are consistent with their predicted colours given their luminosity-weighted ages and metallicities available in the literature. The mean ages derived from the integrated colours of two Local Group dwarf galaxies are consistent with the star formation histories inferred from their resolved stellar populations.

A number of studies have compared properties of galaxies in clusters and in the field to constrain the environmental effects on galaxy properties (e.g. Rose et al. 1994; Terlevich & Forbes 2002; Thomas et al. 2005; Sánchez-Blázquez et al. 2006). A complementary approach to investigate the environmental processes is to compare the properties of galaxies at different radii from the cluster centre (e.g. Guzmán et al. 1992; Carter et al. 2002; Smith et al. 2006, 2008). In hierarchical clustering simulations, the average accretion epoch of subhaloes in cluster-sized parent haloes appears to be correlated with their final radius from the cluster centre (Gao et al. 2004). Gao and his collaborators have found that galaxies within 20 per cent of the virial radius at the present epoch were accreted ~ 8 Gyr ago, while those at the virial radius entered the cluster only ~ 4 Gyr ago. Independently of the precise nature of physical mechanism(s) that suppress star formation in the cluster environment and the timescales involved, the gradual accretion of galaxies into the cluster would likely lead into cluster-centric gradients in the stellar population properties is expected.

In the present paper, we will examine the properties of galaxies in the nearby cluster Abell 1367 by determining the luminosity-weighted ages and metallicities of the dominant stellar populations of Abell 1367 galaxies, and the cluster-centric gradient of galaxy properties. The layout of the paper is as follows. In section 2, we first describe briefly the data set employed and the selection of the sample of the cluster members, while in section 3 we present the relationships between the stellar mass and luminosity-weighted stellar population properties of our sample, and determine the radial trends followed by the properties of the cluster galaxies. Finally, our principal conclusions are represented in section 5.

2 DATA AND SAMPLE SELECTION

The observations, the data reduction techniques applied to the multi-wavelength data set used in the present paper and the selection of the final galaxy sample will be described elsewhere. We therefore only briefly summarize this information here.

Our photometric and spectroscopic observations of the Abell 1367 cluster were taken from a number of facilities. UBR broad-band imaging and narrow-band imaging observations over three pointings of the Wide Field Camera on the INT, i.e., 34×90 arcminute square, were obtained. The exposure times on U-band and B-band filters were 3×300 and 3×150 seconds respectively. The R-band images were taken with an exposure time of 300 seconds, whereas the narrow-band [SII] filter images were obtained for 3×400 seconds. This narrow-band filter was used as it samples the Hα emission at the distance of Abell 1367. The narrow-band filter used includes both Hα and the adjacent [NII]λ6548, 6583 emission lines. For the rest of the paper, we will refer to this only as Hα. J and K broad-band imaging data were

obtained using the Wide Field Camera on UKIRT, covering 0.75 square degrees, centered on the cluster centre.

All photometric data were reduced by the Cambridge Astronomical Survey Unit, with standard pipelines for INT/WFC and UKIRT/WFCAM imaging data. As there are not many standard stars for zero-point calibration in the observed fields, we have used published galaxy photometry as photometric standards. Magnitudes quoted in specific apertures were preferred for this calibration. The zero-points in INT/WFC U-band and B-band photometry used apertures sizes given in Buta (1996). The zero-point for the R-band photometry was calibrated using the photometric data from de Vaucouleurs & Longo (1998) and Taylor et al. (2005). Near-IR imaging data were calibrated using the Two Micron All Sky Survey photometry. Photometry was corrected for foreground Galactic extinction using the reddening maps of Schlegel et al. (1998). We have not attempted to correct the photometry for internal extinction. K-correction, as determined by Poggianti (1997), was applied for all images in all filters. The INT/WFC B-band images were used to visually classify the morphologies of the galaxies in our sample. Signs of disturbance were defined for the sample galaxies that have clear structures, but show i.e. asymmetries, bridges/tails, broken spiral arms, or merger-like morphologies.

To select a sample of likely members of the cluster, we have proceeded as follows. The sample selection started from Hα detections within the central area of the cluster. 86 emission line objects with signal-to-noise larger than five are detected. In order to remove the contamination from foreground stars, objects with full width half maximum smaller than seven pixels, i.e., 5σ above the stellar mean, were excluded. The emission line sample was used to estimate the B-band magnitude limit of galaxies for which Hα emission could be detected. Objects in this sample are all brighter than B=21 magnitude in B-band. This magnitude was adopted as the faint limit of our sample. These criteria were applied to all extended objects

In order to minimise the contamination from background objects, the surface number densities of galaxies were used to estimate the cluster radius and the probable fraction of cluster members. The surface number density of objects brighter than 21 and full width half maximum smaller than seven pixels, is found to drop around half of the Abell radius of the cluster, and these objects are distributed uniformly beyond this radius. Bright objects appear in higher proportion within this radius. We have then decided to consider only galaxies within half of the Abell radius. Then the selection of galaxies was limited by a diameter criterion to optimise the selection of true cluster members. The final selected sample of cluster galaxy candidates comprised 304 galaxies. For these galaxies, isophotal R_{24} apertures were determined to measure UBRJK magnitudes and Hα fluxes.

To determine the cluster membership for galaxies in the photometrically selected sample, spectroscopic observations from the WYFFOS fibre-fed spectrograph on the William Herschel Telescope were obtained to determine their redshifts. The total area covered by WYFFOS/WHT observations covers approximately the same field as the INT/WFC imaging observations, with exposure times of 4×1800 seconds for four pointings and 3×600 seconds for one pointing. The grating used gives a spectral dispersion of approximately 3 $\mathring{\mathrm{A}}$ pixel^{-1}, with a total coverage of 3000 $\mathring{\mathrm{A}}$, centred on 6000 $\mathring{\mathrm{A}}$, covering a number of absorption and emission lines. The observations targeted preferentially faint, blue, and small angular size galaxies in the photometrically selected sample. The faintest object has a total B-band magnitude of 22, and most of the targeted objects are brighter than 21.5 in R-band. The spectroscopic data were reduced using the WYFRED package, a special pipeline for the reduction of multifibre spectroscopy obtained by WHT/WYFFOS. Bias-substracted, median-combined science frames for each pointing, and arcs and sky images used as input for the WYFRED package. The redshifts measured from several lines were averaged for each galaxy. Among the 304 galaxies selected from broad-band photometry data, 128 galaxies have measured redshifts. 72 among them are associated with the Abell 1367 cluster, whereas 56 are background objects. The new cluster members have velocities within 2.5 times the velocity dispersion from the average velocity of the cluster as determined by Struble & Rood (1999). Most of galaxies with spectroscopically determined membership lie within approximately half of the Abell radius of the cluster. The B-band magnitudes of the cluster members range from 16 to 20, with all galaxies brighter than 16 magnitudes in the photometrically selected sample being cluster members. The fraction of cluster members to the known redshift galaxies decreases dramatically from $\sim 80\%$ for galaxies with B-band magnitude ranging from 16 to 17, to 10% for galaxies with magnitude between 19 and 20.

The observed properties of the final sample of Abell 1367 used in the rest of the paper are given in the first five columns of Table 1, giving the galaxy name (column 1), the morphological type (column 2), the presence of morphological disturbance (column 3; y: yes, n: no), and optical/near-IR colours (column 4 and 5).

3 STELLAR POPULATION PROPERTIES OF ABELL 1367 GALAXIES

3.1 Colour-magnitude and colour-colour diagrams

Figures 1 and 2 show the distribution of the galaxies in our sample in four optical/near-IR colour-magnitude diagrams. The galaxies in both figures are coded on the basis of their morphological type, equivalent width of the Hα emission line and the presence of morphological disturbance. These illustrate the wide range in luminosity covered in our analysis, nearly six magnitudes, with galaxies with different properties spread across this range, except the brightest two galaxies which are ellipticals. The colour-magnitude diagrams of our sample galaxies show the normal bimodal structure, in Abell 1367 the blue sequence of late-type galaxies is clearly visible, in agreement with previous studies of this cluster (Godwin & Peach 1982), but in contrast to the colour-magnitude diagrams of more relaxed clusters such as Coma Terlevich et al. (e.g. 2001). Specifically Terlevich et al. (2001) find that most spiral, irregular, and unclassified galaxies in their Coma sample lie on the same (U-V) colour-magnitude relation as the early-type galaxies, with a small fraction populating the blue sequence. In contrast, for our Abell 1367 sample, only two of the 17 galaxies with late-type morphologies have colours consistent with the

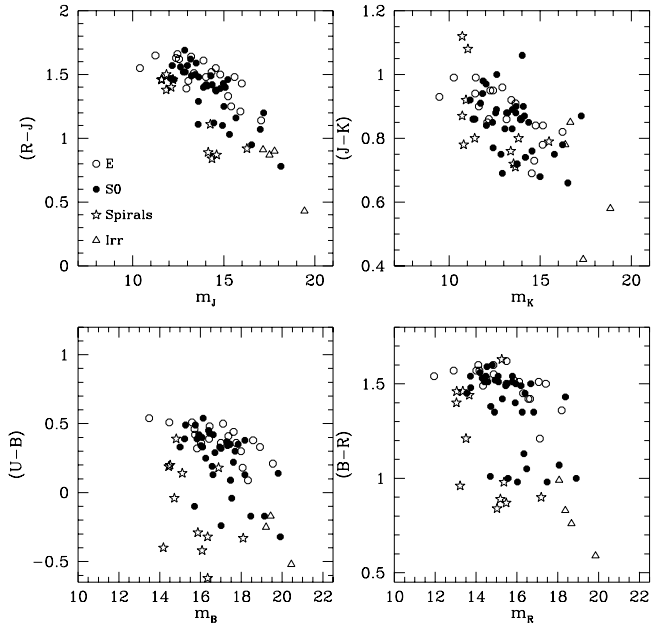

Figure 1. Colour-magnitude relations for our sample with galaxies separated by morphological type.

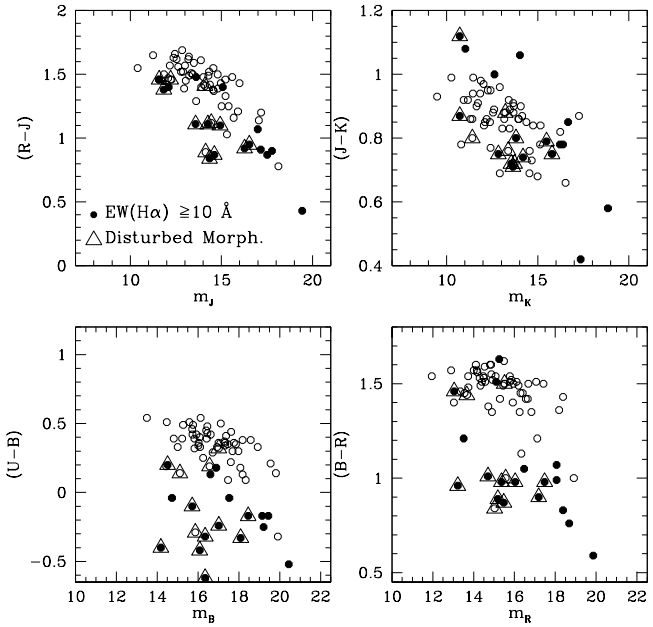

Figure 2. Similar to figure 1, but galaxies are separated by Hα emission line equivalent width and the presence of signs of disturbance.

red sequence, one of which has an Hα emission line equivalent width larger than 10 Å. The bimodality is less clear in the near-IR colour-magnitude diagrams as the near-IR is less sensitive to recent and ongoing star formation.

Interestingly, a number of lenticular galaxies in our sample show Hα emission and blue optical/near-IR colours, and exhibit signs of morphological disturbance, belonging thus to the blue cloud.

Figure 3 shows the distribution of our sample of Abell 1367 galaxies in the (B-K) vs. (J-K) colour-colour diagram, separated by morphological type (upper left panel), integrated stellar mass (upper right panel), equivalent width of Hα emission and signs of the presence of morphological disturbance (lower left panel), and cluster-centric radial distance (lower right panel). In order to convert the photometric information into constraints on the underlying ages and metallicities of the stellar populations, the optical/near-IR photometry must be compared with predictions of stellar population synthesis models. In the simplest version of such models, commonly termed simple stellar populations, all stars are assumed to originate from a single star formation event and thus to have identical chemical compositions and ages. Theoretical predictions for such stellar populations from the models of Pietrinferni et al. (2004) are overplotted on Fig. 3. The grid of models is built assuming a Kroupa (2001) initial mass function, and solar α-to-iron ratio. The models span a wide range of ages, i.e., 0.5, 1., 3., 5, 10 and 14 Gyr, and initial metallicities, i.e., [Fe/H]=-2.27, -1.27, -0.66, and 0.06. Models of constant age are the solid lines, while models of constant metallicity are dotted lines. As clearly shown in the figure, the combination of optical and near-IR colours is able to disentangle the effects of age and metallicity. A comparison of the model grid and the observed colours of our sample shows good agreement between the regions of the colour-colour plane populated by the observations and those where galaxies are expected to lie on the basis of the stellar population synthesis models. By interpolating from the position on the optical/near-IR colour-colour diagram, it is possible to derive the ages, metallicities of the dominant stellar populations, and their associated errors.

By comparing the location of the sample galaxies in the colour-colour diagram to predicted colours, a number of features emerge. The dominant feature in the colour-colour diagram is a tight locus of points in the grid region corresponding to the oldest and most metal rich stellar population models. These galaxies are typically the brightest elliptical and lenticular galaxies in the cluster. Their locus traces what appears to be a metallicity sequence, spanning a range of more than one dex in metallicity at a narrow age range, i.e., ~ 13 Gyr (although the uncertainties in the metallicities and the relative calibration of the colours and grids means that one has to view the ages as defined on a relative, rather than an absolute scale). There is a tendency for these red sequence galaxies to lie above the grid, with rather redder (B-K) colours than predicted by the models even for the oldest ages. One possible explanation for this is the effect of atomic diffusion in stellar interiors. Such gravitational settling of helium and heavier elements has been demonstrated to occur in the Sun (Guenther 1994) but its occurrence in old stellar populations such as globular clusters is uncertain (Gratton et al. 2001; Korn et al. 2006). As a result, this effect is not included in the BaSTI models. If it were to be included, the model grid would extend to redder (B-K) colours for old stellar populations.

In contrast with the elliptical galaxies, for which the low mass objects appear to extend the metallicity sequence defined by the brighter ellipticals to low stellar metallicities, the optical/near-IR colours of less massive lenticular galaxies

show a different colour-colour relationship, consistent with the appearance of a population of lenticular galaxies with young luminosity-weighted mean ages and low stellar metallicities.

Another prominent feature in the colour-colour diagram is the presence of a population of galaxies with optical/near-IR colours consistent with those of synthetic stellar populations of young ages and low metallicities. None of the ellipticals belongs to this group of galaxies. All members of this population belong to the blue cloud as defined in the colour-magnitude diagrams (Fig. 1 and Fig. 2). All are disturbed morphologically with ongoing star formation activity. Their stellar masses can be as high as those of galaxies in the tight metallicity sequence populated by old and passive red sequence galaxies, and extend down to lower masses.

A small number of galaxies in our sample show very red (J-K) colours, and lie well outside the grid of models. One of them is UGC 6697, a well studied system of what appears to be a merger of two edge-on galaxies (Gavazzi et al. 2001), accompanied by a vigorous star forming event with Hα emission equivalent width of 94 Å. The geometry of the system suggests that the photometry could be severely affected by internal reddening. The second object is G1143498+195835, a low mass lenticular, which lies close to UGC 6697, with a projected distance of ~ 7 kpc. Despite the ongoing ram pressure gas stripping (Boselli & Gavazzi 2006), there is apparently still a sufficient gas reservoir in this galaxy to sustain a star formation event, with a measured Hα emission line equivalent width of 31 Å. The third object is UGC 6702, a bright spiral galaxy with circumnuclear star formation, and Hα equivalent width of 32 Å. For the last two objects, the red (J-K) colour and the intermediate (B-K) colour could be interpreted as a possible signature of the presence of a sizeable population of red intermediate mass carbon stars. Additional near-IR spectroscopy could help understanding the optical/near-IR photometric properties of these objects.

3.2 Single metallicity vs. multi-metallicity synthesis models

Galaxies are known to have experienced complex chemical evolution and star formation histories. To check if our choice of comparing galaxy colours to a grid of single age and single metallicity stellar population models is biasing our results, we compare the optical/near-IR colours of the sample galaxies to a grid of models based on the chemical evolution scenario recently presented in Schombert & Rakos (2009a). This model assumes that galaxies are a sum of single stellar populations of metallicities following the infall scenario tuned to match the shape of the metallicity distribution functions of the Milky Way and NGC 5128. The metallicity distribution is allowed then to slide in the peak metallicity to produce a range of total metallicities per galaxy age. Each model produces a metallicity value based on the luminosity weighted average of each metallicity bin (see Schombert & Rakos 2009a, for a full description of the chemical evolution scenario).

The upper panels of Fig. 4 show the comparison between a grid of stellar population synthesis models based on Schombert & Rakos (2009a) chemical evolution scenario and the distribution of optical/near-IR colours of our sample galaxies. Galaxies are separated by stellar mass and equivalent width of Hα emission (upper left panel), and morphological type (upper right panel). The overall features emerging from the comparison between the observed galaxy colours and the predicted grid are comparable to those noticed when the former were compared to the grid of simple stellar population models. The sequence of early-type galaxies, the population of intermediate age lenticular galaxies, and the population of (generally low mass) galaxies dominated by young stellar population are seen again. A careful comparison indicates, however, that differences exist. At a given age and metallicity, the multi-metallicity models tend to predict bluer colours than their equivalent BASTI models. This is due to the inclusion of a metal-poor tail that contribute more to colour than mean metallicity. The colours of the sample galaxies are then matched by models of higher metallicities and younger ages than when compared to predictions of single stellar population models.

The lower panels of Fig. 4 show comparisons between the ages (lower left panel) and metallicities (lower right panel) of the sample galaxies derived by using the BASTI models and multi-metallicity models respectively. As suspected, the ages derived using the BASTI models are much older than those derived using the multi-metallicity models. When the latter models are considered, more than half of quiescent elliptical galaxies in the sample are predicted to be dominated by stars of young to intermediate ages, i.e., 2-5 Gyr. This is surprising as the chemical evolution scenario of Schombert & Rakos (2009a) was introduced to support the case that early-type galaxies on the red sequence are systematically old (see Schombert & Rakos 2009a, for a detailed discussion).

Multi-metallicity stellar population models are found to over-estimate galaxy metallicities by a factor of about three compared to those derived using the BASTI models, over the entire metallicity range covered by passive galaxies in the sample. This is expected as the young ages found for elliptical galaxies using those models require solar to super-solar metallicities to explain their colours. Differences in estimated metallicities for galaxies with ongoing star formation activity are even larger, up to about 1 dex at the metal-poor end of the metallicity range covered by the sample galaxies. This is due to the combined contribution of bright and blue young stars that dominated the light of those objects, and to the presence of blue stars populating the metal-poor tail of the metallicity distribution.

Despite those differences in the predicted ages and metallicities, the overall features of the distribution of the sample galaxies in the diagnostic diagrams discussed below are, however, reassuringly similar. As stellar population parameters derived by comparing galaxy colours to single stellar population synthesis models s have a straightforward interpretation, and due to the uncomfortably young ages of galaxies estimated when using the multi-metallicity models, we have decided to use the ages and metallicities derived using the BASTI models for the rest of the paper.

As galaxies contain mixed stellar populations in term of their ages and metallicities, the estimated stellar population properties by comparing their broad-band colours to those of synthetic single stellar populations will be luminosity-weighted mean values. Integrated galaxy stellar masses are estimated using the mass-to-light ratio vs. colour calibra-

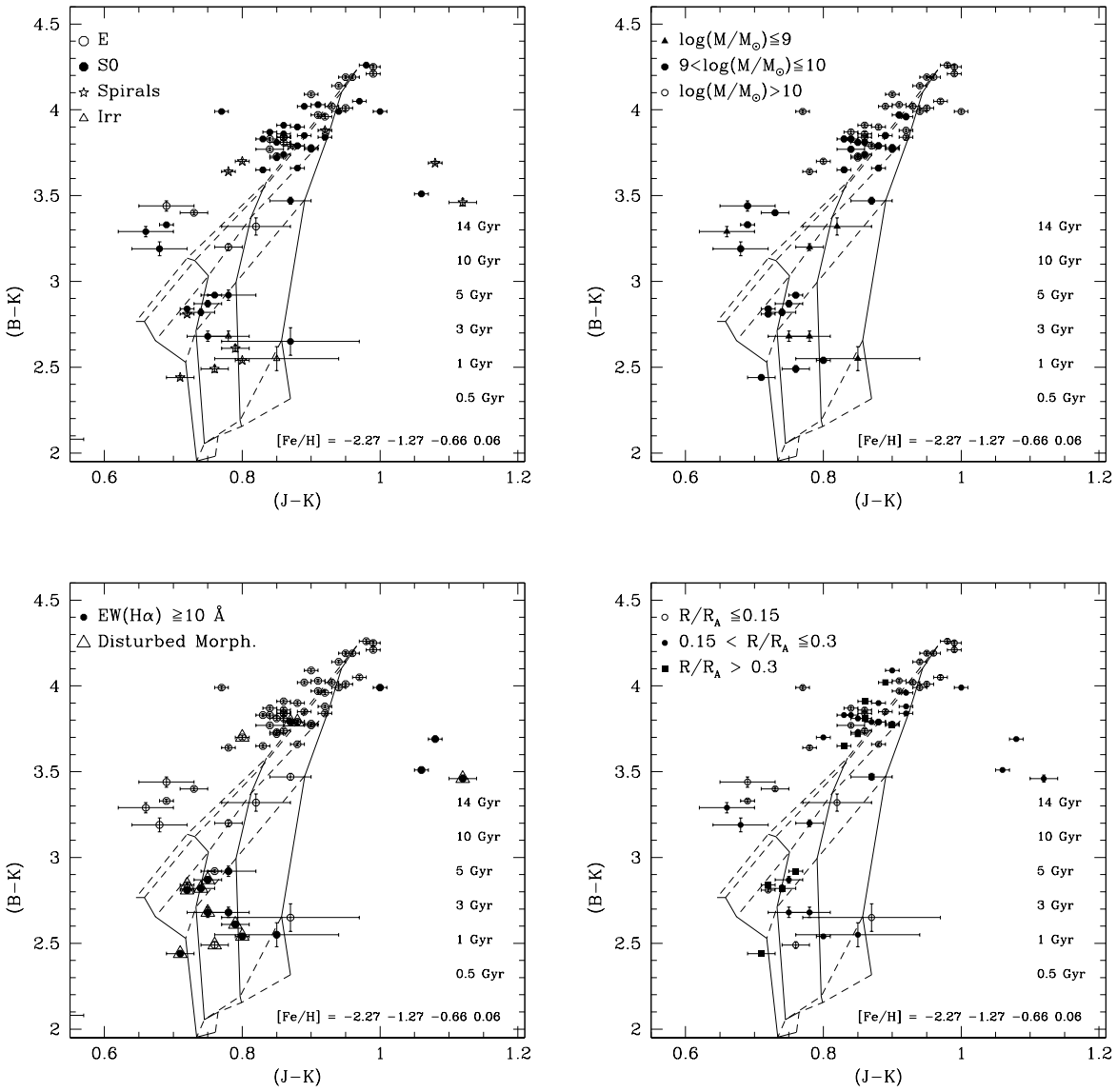

Figure 3. Optical/near-IR colour-colour diagrams for the sample of galaxies studied in the present paper separated by morphological type (the upper-left panel), stellar mass (the upper-right panel), equivalent width of Hα emission and the presence of morphological disturbance (the lower-left panel), and cluster-centric distance (the lower-right panel). Overplotted are the Pietrinferni et al. (2004) stellar population models for a simple stellar population. Solid and dashed lines connect models of constant metallicities and ages, respectively.

tion of Bell & de Jong (2001). These authors have argued that the stellar masses derived from their relation are robust against the effect of dust provided the dust vectors are parallel to the relation. The reason is that the under-estimate of stellar mass arising from the attenuation in luminosity will be compensated by the overproduction of stellar mass arising from the reddening in colour, therefore yielding comparable final stellar masses. This balance might apply for face-on systems, but could not be the case for highly inclined systems as the latter show a systematically higher ratio of attenuation to reddening. The overall consequence is that stellar masses could be under-estimated for a randomly oriented distribution by the use of the Bell & de Jong (2001) colour vs. mass-to-light ratio if dust is not taken into account. Driver et al. (2007) have explored this in detail, and concluded that while the masses are modified somewhat the final stellar mass breakdown is not dramatically altered. The last three columns of Table 1 give the integrated stellar masses, the luminosity-weighted ages, and the luminosity-weighted metallicities for our sample of Abell 1367 galaxies.

3.3 Stellar mass-metallicity relation

Figure 5 shows the relationship between the luminosity-weighted age and the integrated stellar mass for our sample of Abell 1367 members. Galaxies are separated by mor-

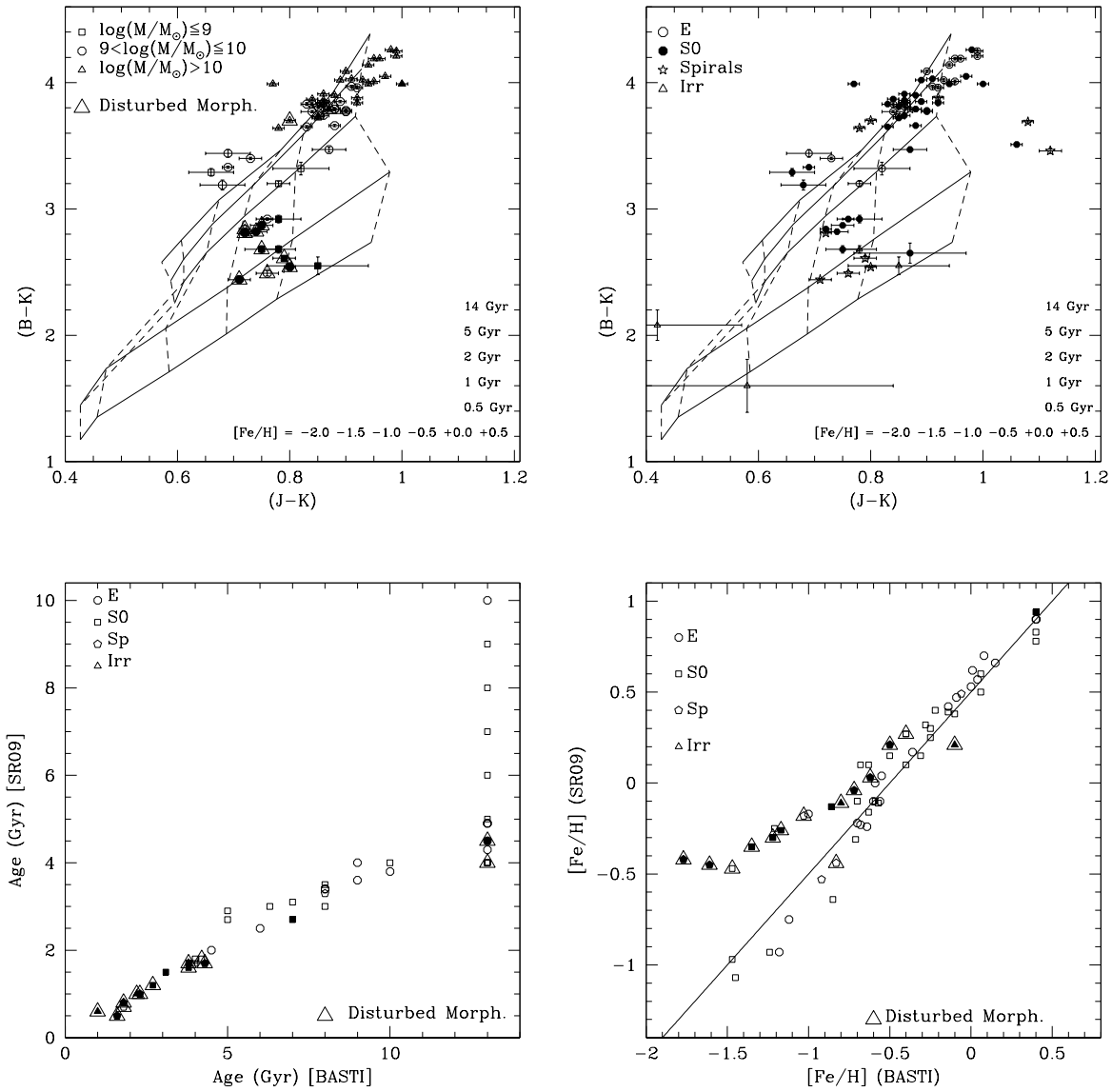

Figure 4. Comparison between derived stellar population properties of the sample galaxies using respectively a grid of simple stellar population models and a grid of models based on the chemical evolution scenario of Schombert & Rakos (2009a). The upper panels show the optical/near-IR colour-colour diagrams for the sample galaxies compared to the grid of models based on Schombert & Rakos (2009a) chemical evolution scenario. Galaxies are separated by stellar masses (the left panel), with filled symbols showing galaxies with equivalent width of Hα larger than 10 Å, and morphological type (the right panel). The lower panels show comparisons between the derived ages (left panel) and metallicities (lower panel) of the stellar populations of the sample galaxies. Filled symbols show galaxies with equivalent width of Hα larger than 10 Å. The solid line shows the relation $[Fe/H]_{SR09}=[Fe/H]_{BASTI}+0.5$.

phological type in the upper left panel, equivalent width of Hα emission line and the presence of signs of morphological disturbance in the upper right panel, and the cluster-centric distance normalized to the cluster Abell radius in the lower panel. As suspected from the distribution of galaxies in the optical/near-IR colour-colour diagram, elliptical galaxies show uniformly old ages across a factor of more than 100 in integrated stellar mass. Out of the sub-sample of ellipticals, two objects stand out as their stellar contents appear to be dominated by populations of much younger luminosity-weighted ages, i.e., ~ 5 Gyr. The population of lenticular galaxies exhibits however a much clearer age vs. stellar mass relationship, extending from ages typical of old elliptical galaxies to young ages typical of those of late-type galaxies with young luminosity-weighted ages. Galaxies in the blue cloud, which are presently actively forming stars, show all young luminosity-weighted ages. The bulk of those galaxies are located at cluster-centric distances larger than 20 per cent of the Abell radius of the cluster.

Fig. 6 shows the relationship between the luminosity-weighed metallicity and the integrated stellar mass for our sample of Abell 1367 members. Galaxies are separated by

morphological type (upper left panel), equivalent width of Hα emission line and the presence of signs of morphological disturbance (upper right panel), luminosity-weighted age (lower left panel), and the cluster-centric distance normalized to the Abell radius of the cluster (lower right panel). A clear trend between luminosity-weighted metallicity and stellar mass is apparent, in agreement with previous results for both field (e.g. Gallazzi et al. 2005) and cluster galaxies (e.g Nelan et al. 2005). The luminosity-weighted stellar metallicity of Abell 1367 galaxies increases with stellar mass, from roughly 10 per cent of solar for galaxies with stellar masses below 10^9 M$_\odot$ to about 2.5 times solar for those with stellar masses $\sim 10^{11}$ M$_\odot$. The scatter is clearly greater than the observational uncertainties, suggesting that the stellar mass is not the sole parameter that shapes the chemical histories of galaxies. For galaxies in the red sequence, neither age nor morphological type seem to be a factor in the relationship between integrated stellar mass and luminosity-weighted metallicity, as old elliptical galaxies cover a similar range in metallicity as lenticular galaxies which exhibit a spread in luminosity-weighted ages, and both populations have similar metallicity dispersions. Linear fits to red sequence elliptical and lenticular subsamples show that the slopes and the normalizations of the separate relationships are consistent with each other within the errors.

Galaxies with ongoing star formation activity and/or with late-type morphological types show a different behaviour, however. They tend to have luminosity-weighted metallicities lower than those of the red sequence galaxies with similar integrated stellar masses. To investigate this further, Fig. 7 shows the relationship between the residual from the linear least square bisector fit of the stellar mass-metallicity relation of the entire galaxy sample as a function of (U-K) colour (lower right panel), luminosity-weighted ages and morphological type (lower left panel), star formation rate (upper right panel), and Hα emission line equivalent width (upper left panel). Galaxies with disturbed optical morphologies are marked by large open triangles in all panels. Apart from the lower left panel, galaxies with luminosity-weighted ages younger than 5 Gyr are shown as open circles, older galaxies are displayed as filled circles. The star formation rates were estimated using the Hα flux and the calibration of Kennicutt (1998). Fluxes were not corrected for either galaxy internal reddening nor from contamination from [NII]λ6548, 6583 emission line. It can be clearly seen that the bulk of galaxies with disturbed morphologies and ongoing star formation, i.e., blue cloud galaxies, lie below the stellar mass-metallicity relation of the sample. No clear trend between the residuals from the stellar mass-metallicity and galaxy colour, mean age, emission line equivalent width, or star formation rate is apparent, suggesting none of them is driving alone the scatter around the stellar mass-metallicity relation.

The bulk of blue cloud galaxies in our sample exhibit disturbed morphologies. The observed tendency of blue galaxies in the cluster to be chemically underabundant relative to passive old galaxies in the red sequence could result from gas inflow induced by tidal interactions and/or minor mergers. The star formation activity associated with disturbed galaxies indicates that those galaxies still retain a substantial amount of gas which may be expected to be

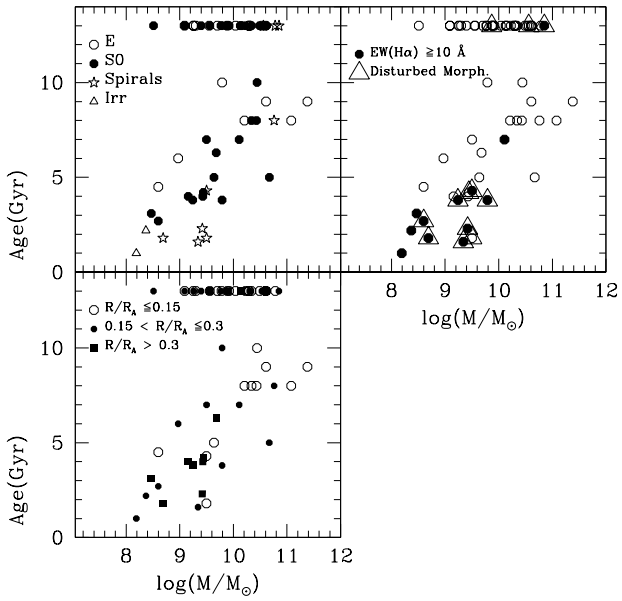

Figure 5. The relationship between the luminosity-weighted stellar age and the stellar mass for our sample with galaxies separated by morphological type (upper left panel), Hα emission line equivalent width and the presence of signs of disturbance (upper right panel), and radial distance (lower panel).

stripped by ram-pressure and/or harassment effect by extended exposure to the cluster environment. Moss (2006) has found for an ensemble cluster formed from eight low-redshift clusters, that the majority of the infall galaxy population are in interacting or merging systems characterized by slow gravitational encounters. Merger numerical simulations predict gas inflows to occur in galaxy interactions (e.g. Mihos & Hernquist 1996; Barnes 2002). Radial abundance gradients exist in most disk galaxies, such that gas phase metallicity decreases with increasing distance from the galactic centre (e.g. Zaritsky et al. 1994). If gas inflows have triggered the star formation events as expected (e.g. Barnes & Hernquist 1996), then those gas inflows may have carried less enriched gas from the outer regions of the galaxy, diluting the chemical abundances of the star-forming gas, thus lowering the metallicities of young stars. The recent numerical simulations of equal-mass mergers of Rupke et al. (2010) confirm the hypothesis that merger-driven radial inflow of low metallicity gas from the outskirts of the interacting galaxies produce a dilution of nuclear abundances of interacting galaxies (see also Montuori et al. 2010). The recent observations of Kewley et al. (2010) indicate indeed that the metallicity gradients for a sample of interacting galaxies are systematically shallower than for non-interacting galaxies. The interaction-induced gas inflow scenario was proposed to explain the offset of different classes of interacting/merging galaxies from the luminosity/mass-metallicity relationship of non-interacting galaxies. Kewley et al. (2006) and Michel-Dansac et al. (2008) have shown that the interstellar gas of nearby optically-selected close galaxy pairs in the field is underabundant when compared to local star-forming galaxies of

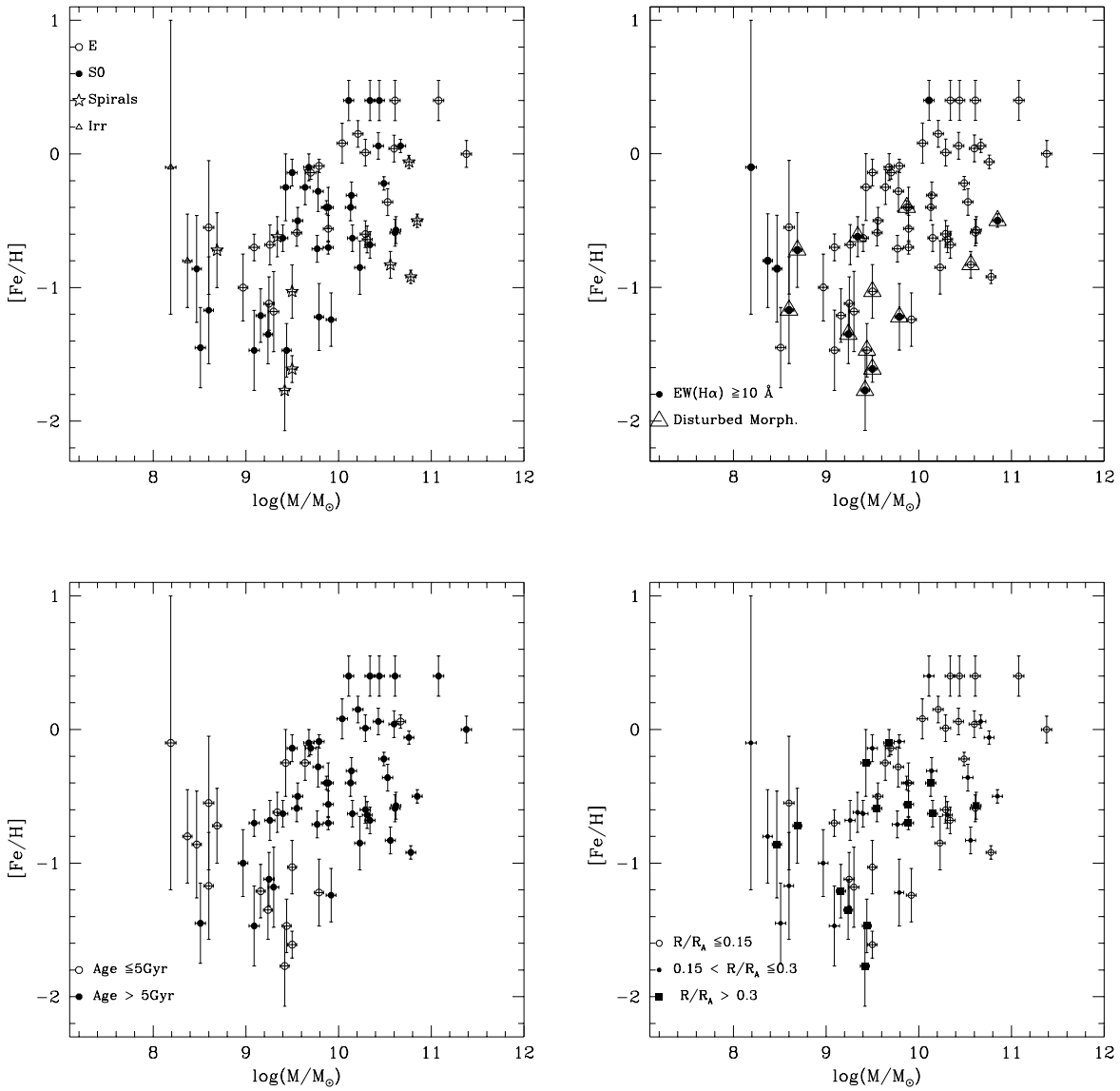

Figure 6. The relationship between galaxy luminosity-weighted stellar metallicity and stellar mass for our sample with galaxies separated by morphological type (upper left panel), Hα emission line equivalent width and the presence of signs of disturbance (upper right panel), luminosity-weighted stellar age (lower left panel), and cluster-centric distance (lower right panel).

similar luminosities and stellar masses. The offset from the gas phase metallicity-luminosity for non-interacting galaxies appears to depend on the projected separation between the interacting galaxies and the burst strength (Kewley et al. 2006). Peeples et al. (2009) have identified a sample of metal-poor high-mass outliers from the local gas-phase mass-metallicity relation. These galaxies are found to exhibit disturbed morphologies, blue colours, and high star formation rates for their masses, implying that they are undergoing tidal interactions. Similarly, Rupke et al. (2008) have found that the interstellar gas of local luminous infrared galaxies is underabundant. The offset in abundance from the gas phase oxygen abundance vs. luminosity/mass relation is found to correlate with the total infrared luminosity, with a larger offset for ultra-luminous infrared galaxies than for luminous infrared galaxies. The offsets from the mass vs. gas phase metallicity relation in optically selected mergers is lower than for luminous and ultra-luminous infrared galaxies, suggesting that the offset from the properties of non-interacting galaxies depends on the strength and the stage of the interaction. The modest offset from the stellar mass-metallicity relation we observe for disturbed galaxies in the blue cloud sequence of Abell 1367 could reflect a continuation of the trends observed for equal-mass mergers to lower strength of galaxy interaction. Measuring gas phase metallicities of star-forming galaxies in our sample to compare with those of both morphologically undisturbed star-forming galaxies, and strongly disturbed galaxies would test this scenario.

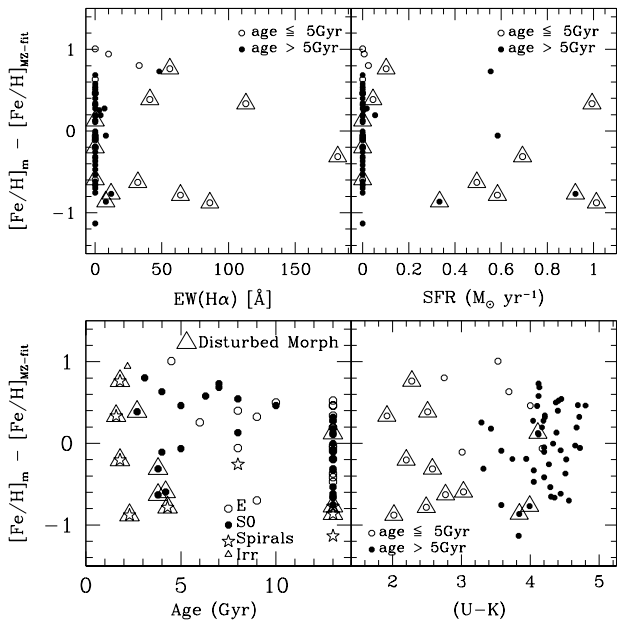

Figure 7. Difference between the measured stellar metallicity and the stellar mass-metallicity relation as a function of the luminosity-weighted age (lower left panel), (U-K) colour (lower right panel), Hα emission line equivalent width (upper left panel), and star formation rate (upper right panel), respectively.

3.4 Radial dependence of stellar population properties

For a cluster survey, the projected cluster-centric distance is a convenient parameter to describe the environment of a galaxy, although it may not be entirely free from introducing potential biases (see Lane et al. 2007). In this section, we examine the dependence of stellar population properties of the cluster galaxies on the distance of the galaxy from the cluster centre, which has been taken to be at R.A.(J2000)=$11^h44^m29.5^s$ and dec(J2000)=$+19^\circ50'21''$. We express the cluster-centric radius in terms of the cluster Abell radius, taken to be $80'$.

Figure 8 shows the relationship between the cluster-centric radial distance, normalised to the Abell radius of the cluster, and the integrated stellar mass (left panel), the luminosity-weighted stellar metallicity (middle panel), and the residuals from the bisector fit of the stellar mass-metallicity relations (right panel). Galaxies in the sample are separated between those in the red sequence, shown as filled circles, and those in the blue cloud, shown as open circles. Galaxies that show signs of the presence of morphological disturbance are flagged with large open triangles. The residuals for each subsample are estimated using the linear least square bisector fit to the mass-metallicity relation of the subsample. In each panel, the solid line shows the best linear fit for red sequence galaxies, while the dashed line shows the fit to galaxies in the blue cloud. All galaxies are assigned equal weight in the fits, since the scatter is primarily intrinsic and the measurement errors similar for the bulk of the points. The slopes and the associated errors of the fit to the cluster-centric radial gradients are indicated for both subsamples.

As expected, more massive red sequence galaxies lie preferentially in the core of the cluster. As red sequence galaxies exhibit a clear mass-metallicity relation, a strong negative luminosity-weighted metallicity gradient as a function of the cluster-centric distance is present. The metallicity residuals for these galaxies do not show however a statistically significant correlation with the cluster-centric galaxy distance. Because the stellar populations of the cluster red sequence galaxies follow scaling relations with stellar mass, the residuals from these relations are comparing the inner and outer galaxy population at fixed stellar mass. On average, red sequence galaxies at 40 per cent of the Abell radius of the cluster are $\sim 0.49 \pm 0.28$ dex poorer than galaxies of similar stellar masses in the cluster core. Similarly, blue cloud galaxies show a negative stellar mass gradient, however the luminosity-weighted metallicity shows no significant correlation with the cluster-centric radius. The residuals from the luminosity-weighted metallicity-mass relation of star-forming galaxies show no statistically significant correlation with the projected distance from the cluster centre. The lack of a negative correlation for the star forming galaxies could be caused by enhanced star formation, leading to lower luminosity-weighted metallicities (see section 3.3 above) in higher density regions of the cluster as compared with lower density regions (see Moss et al. 1998; Moss & Whittle 2000). Alternatively, given the small size of the our sample, projection effects could cause a dilution of the expected gradients, although such dilution effects are expected to be small in the sampled region within half the Abell radii (Moss et al. 1998).

Finally, neither red sequence galaxies nor star-forming galaxies show cluster-centric radial gradients for the residual from the relationship between luminosity-weighted age and stellar mass, over the radial range covered by the sample galaxies.

Ellipticals and lenticulars populating the red sequence do appear to be dominated by different stellar populations (see Fig. 3 and 5), suggesting that they might have experienced different assembly histories. It is legitimate then to check how their stellar population properties taken separately change radially within the cluster. Figure 9 shows the relationships between the cluster-centric distance normalized to the Abell radius of the cluster and the residuals from the stellar mass-metallicity relations (the upper panel) and the stellar mass-age relations (the lower panel) for ellipticals and lenticulars in the red sequence shown as open and filled circles respectively. The fits to the stellar mass vs. metallicity/age relations are done separately for elliptical and lenticular subsamples. The slopes and their associated errors of the best linear fits to the relations between the residuals and the normalized cluster-centric radial distance are indicated. No statistically significant trends are found between the residuals from the mass-metallicity/mass-age relations and the cluster-centric galaxy distance for neither red sequence ellipticals nor lenticulars. This indicates that no significant differences in the mean luminosity-weighted metallicities and ages are present, at a fixed stellar mass, between the red sequence galaxy sub-populations distributed within the 40 per cent of the Abell radius of the cluster covered by our survey. The lack of age differences between red

Table 1. Properties of our sample of Abell 1367 galaxies

SDSS-ID	Type	Dis.	(B-K)	(J-K)	log ($M/M_{\odot}$)	Age (Gyr)	[Fe/H]
J114229.18+200713.7	Irr	n	2.08 ± 0.12	0.42 ± 0.15			
J114239.31+195808.1	Sc	y	2.61 ± 0.02	0.79 ± 0.02	8.69 ± 0.05	1.8 ± 0.3	-0.72 ± 0.28
J114240.34+195717.0	S0	n	2.92 ± 0.03	0.78 ± 0.04	8.47 ± 0.05	3.1 ± 1.5	-0.86 ± 0.4
J114246.11+195654.6	E	n	3.84 ± 0.01	0.86 ± 0.01	9.89 ± 0.05	13 ± 2	-0.56 ± 0.1
J114251.93+195657.0	S0/a	n	2.92 ± 0.01	0.76 ± 0.01	9.16 ± 0.05	4 ± 0.5	-1.21 ± 0.2
J114253.19+201045.9	S0/a	n	3.77 ± 0.01	0.9 ± 0.01	9.68 ± 0.05	6.3 ± 2	-0.10 ± 0.1
J114256.45+195758.3	Scd	y	2.44 ± 0.01	0.71 ± 0.02	9.42 ± 0.05	2.3 ± 0.2	-1.77 ± 0.3
J114258.69+195612.9	Irr	n	2.55 ± 0.07	0.85 ± 0.09	8.19 ± 0.06	1.0 ± 1.2	-0.10 ± 1.1
J114301.18+195435.2	E	n	3.2 ± 0.02	0.78 ± 0.02	8.97 ± 0.05	6.0 ± 3	-1.00 ± 0.25
J114306.32+195620.3	SB0	n	3.9 ± 0.01	0.88 ± 0.01	10.14 ± 0.05	13 ± 2	-0.31 ± 0.1
J114313.09+200017.3	S,Pec	y	2.54 ± 0.01	0.8 ± 0.01	9.34 ± 0.05	1.6 ± 0.2	-0.62 ± 0.15
J114313.27+200754.8	S0	n	3.47 ± 0.02	0.87 ± 0.03	9.43 ± 0.05	4.0 ± 1	-0.25 ± 0.25
J114317.64+194657.6	E/S0	n	3.96 ± 0.01	0.92 ± 0.01	9.79 ± 0.05	10 ± 3	-0.09 ± 0.05
J114321.95+195705.8	E	n	3.83 ± 0.01	0.84 ± 0.01	9.26 ± 0.05	13 ± 2	-0.68 ± 0.15
J114324.55+194459.3	Sa	n	3.88 ± 0.01	0.92 ± 0.01	10.76 ± 0.05	8.0 ± 1	-0.06 ± 0.05
J114324.88+203327.2	S0	n					
J114336.23+195935.6	S0	n	3.81 ± 0.01	0.85 ± 0.01	9.4 ± 0.05	13 ± 2	-0.63 ± 0.1
J114341.16+195311.1	S0	n	3.78 ± 0.01	0.9 ± 0.01	9.5 ± 0.05	7.0 ± 2	-0.14 ± 0.1
J114341.54+200137.0	S0	y	2.68 ± 0.03	0.75 ± 0.03	8.6 ± 0.05	2.7 ± 0.5	-1.17 ± 0.4
J114343.96+201621.7	S0/a	n	3.91 ± 0.01	0.86 ± 0.01	10.62 ± 0.05	13 ± 2	-0.57 ± 0.1
J114347.75+202148.0	S0	y	2.84 ± 0.01	0.72 ± 0.01	9.44 ± 0.05	4.2 ± 0.6	-1.47 ± 0.2
J114348.89+201454.0	S0	y	2.82 ± 0.02	0.74 ± 0.02	9.24 ± 0.05	3.8 ± 0.9	-1.35 ± 0.22
J114349.07+195806.4	Scd	y	3.46 ± 0.02	1.12 ± 0.02			
J114349.87+195834.8	S0	n	3.51 ± 0.01	1.06 ± 0.01			
J114350.12+195703.1	E	n	3.32 ± 0.05	0.82 ± 0.05	8.6 ± 0.06	4.5 ± 5	-0.55 ± 0.5
J114351.33+195143.6	E/S0	n	3.44 ± 0.03	0.69 ± 0.04	9.3 ± 0.05	13 ± 2	-1.18 ± 0.3
J114353.56+194421.7	S0	n	3.79 ± 0.01	0.88 ± 0.01	9.89 ± 0.05	13 ± 3	-0.4 ± 0.15
J114356.42+195340.4	E	n	4.21 ± 0.01	0.99 ± 0.01	11.08 ± 0.06	8.0 ± 3	0.40 ± 0.15
J114357.44+195608.4	S0	n	3.66 ± 0.01	0.88 ± 0.01	9.64 ± 0.05	5.0 ± 2	-0.25 ± 0.13
J114357.46+201802.0	S0	n	3.72 ± 0.01	0.85 ± 0.01	10.15 ± 0.05	13 ± 2	-0.63 ± 0.1
J114357.50+195713.6	S0	n	4.26 ± 0.01	0.98 ± 0.01	10.44 ± 0.06	10 ± 3	0.40 ± 0.15
J114357.70+201124.1	S0	n	3.19 ± 0.04	0.68 ± 0.04	9.09 ± 0.05	13 ± 2	-1.47 ± 0.3
J114358.09+204822.9	Sa	n					
J114358.23+201107.9	S0	y	2.87 ± 0.02	0.75 ± 0.02	9.79 ± 0.05	3.8 ± 0.6	-1.22 ± 0.25
J114358.83+195330.6	E	n	3.97 ± 0.01	0.91 ± 0.01	9.7 ± 0.05	13 ± 3	-0.14 ± 0.05
J114358.95+200437.2	Sa	n	3.69 ± 0.01	1.08 ± 0.01			
J114359.57+194644.2	SB0	n	4.05 ± 0.01	0.97 ± 0.01	10.34 ± 0.05	8.0 ± 3	0.40 ± 0.15
J114401.94+194703.9	Sc	y	2.49 ± 0.02	0.76 ± 0.02	9.5 ± 0.05	1.8 ± 0.2	-1.03 ± 0.2
J114402.15+195659.3	E	n	4.02 ± 0.01	0.93 ± 0.01	11.38 ± 0.05	9.0 ± 3	0.00 ± 0.1
J114402.15+195818.8	E	n	4.14 ± 0.01	0.94 ± 0.01	10.6 ± 0.05	13 ± 3	0.04 ± 0.1
J114403.02+194424.8	S0	n	3.85 ± 0.01	0.89 ± 0.01	9.78 ± 0.05	13 ± 3	-0.28 ± 0.15
J114403.21+194803.9	E	n	4.01 ± 0.01	0.95 ± 0.01	10.21 ± 0.05	8.0 ± 2	0.15 ± 0.1
J114403.79+200556.1	S0	n	3.83 ± 0.01	0.83 ± 0.01	9.77 ± 0.05	13 ± 2	-0.71 ± 0.1
J114405.46+195945.9	SB0	n	3.86 ± 0.01	0.86 ± 0.01	10.61 ± 0.05	13 ± 2	-0.59 ± 0.1
J114405.74+201453.5	S0	n	4.02 ± 0.01	0.89 ± 0.01	10.13 ± 0.05	13 ± 2	-0.40 ± 0.1
J114407.64+194415.1	E	n	3.84 ± 0.01	0.86 ± 0.01	10.29 ± 0.05	13 ± 2	-0.60 ± 0.1
J114412.18+195633.9	E	n	3.77 ± 0.01	0.84 ± 0.02	9.09 ± 0.05	13 ± 2	-0.70 ± 0.1
J114416.48+201300.7	E	n	4.09 ± 0.01	0.9 ± 0.01	10.53 ± 0.05	13 ± 2	-0.36 ± 0.1
J114417.20+201323.9	Sa	y	3.7 ± 0.01	0.8 ± 0.01	10.56 ± 0.05	13 ± 2	-0.83 ± 0.1
J114418.99+201812.9	E/S0	n	3.81 ± 0.01	0.86 ± 0.01	9.55 ± 0.05	13 ± 2	-0.59 ± 0.1
J114420.42+195851.0	E/S0	n	4.25 ± 0.01	0.99 ± 0.01	10.61 0.06	9.0 ± 3	0.40 ± 0.15
J114420.74+194933.3	SB0	n	4.03 ± 0.01	0.91 ± 0.01	10.49 ± 0.05	13 ± 2	-0.22 ± 0.05
J114422.21+194628.2	E	n	4.19 ± 0.01	0.96 ± 0.01	10.04 ± 0.06	13 ± 3	0.08 ± 0.15
J114425.12+194941.0	S0	n	3.87 ± 0.01	0.84 ± 0.01	10.34 ± 0.05	13 ± 2	-0.68 ± 0.1
J114425.10+200628.1	E	n	3.73 ± 0.01	0.85 ± 0.01	10.31 ± 0.05	13 ± 2	-0.64 ± 0.1
J114425.92+200609.6	S0	y	3.79 ± 0.01	0.88 ± 0.01	9.87 ± 0.05	13 ± 3	-0.4 ± 0.05
J114428.36+194406.6	E	n	4.19 ± 0.01	0.95 ± 0.01	10.29 ± 0.06	13 ± 3	0.01 ± 0.1
J114430.14+201944.5	S0	n	3.65 ± 0.01	0.83 ± 0.01	9.89 ± 0.05	13 ± 3	-0.70 ± 0.05
J114430.55+200436.0	S0	n	3.84 ± 0.01	0.92 ± 0.01	10.67 ± 0.05	5.0 ± 0.8	0.06 ± 0.05
J114432.12+200623.8	S0/a	n	3.99 ± 0.01	1 ± 0.01	10.11 ± 0.05	7.0 ± 5	0.40 ± 0.15
J114436.55+194505.7	S0	n	3.74 ± 0.01	0.86 ± 0.01	9.56 ± 0.05	13 ± 3	-0.50 ± 0.1
J114446.62+194528.3	S0	n	3.99 ± 0.01	0.77 ± 0.01	10.23 ± 0.06	13 ± 2	-0.85 ± 0.2

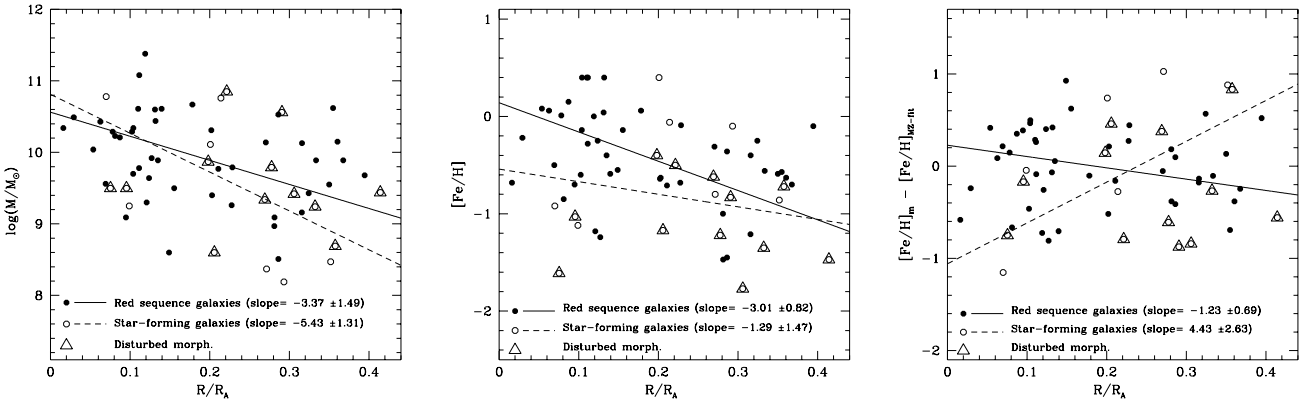

Figure 8. Stellar mass, stellar metallicity, and residual from the stellar mass-metallicity relation as a function of the normalised projected radius for our sample of galaxies. In each panel, the solid line represents the least square bisector fit to the sub-sample of red sequence galaxies shown as filled circles, and the dashed line represents the fit to the sub-sample of blue cloud galaxies shown as open circles. Galaxies which display signs of morphological disturbances are flagged with large triangles.

Table 1. Properties of our sample of Abell 1367 galaxies (continued).

SDSS-ID	Type	Dis.	(B-K)	(J-K)	log (M/M$_\odot$)	[Fe/H]	Age (Gyr)
J114447.03+200730.3	Sbc	y	3.79 ± 0.01	0.87 ± 0.01	10.85 ± 0.05	13 ± 3	-0.5 ± 0.05
J114447.28+201247.4	S0	n	3.29 ± 0.03	0.66 ± 0.04	8.51 ± 0.06	13 ± 2	-1.45 ± 0.3
J114447.44+195234.9	S0	n	3.99 ± 0.01	0.94 ± 0.01	10.43 ± 0.05	8.0 ± 1.5	+0.06 ± 0.1
J114447.79+194624.3	Sc	y	2.81 ± 0.01	0.72 ± 0.01	9.5 ± 0.05	4.3 ± 0.5	-1.61 ± 0.1
J114447.95+194118.6	SB0/a	n	3.33 ± 0.01	0.69 ± 0.01	9.92 ± 0.05	13 ± 2	-1.24 ± 0.2
J114449.16+194742.2	Sa	n	3.64 ± 0.01	0.78 ± 0.01	10.78 ± 0.05	13 ± 2	-0.92 ± 0.05
J114449.62+195627.9	E	n	3.4 ± 0.01	0.73 ± 0.02	9.25 ± 0.05	13 ± 2	-1.12 ± 0.2
J114450.31+195903.7	SB0/a	n	2.65 ± 0.08	0.87 ± 0.1			
J114451.09+194718.2	Irr	n	1.6 ± 0.21	0.58 ± 0.26			
J114452.40+201117.0	Irr	n	2.68 ± 0.03	0.78 ± 0.03	8.37 ± 0.05	2.2 ± 0.5	-0.8 ± 0.35

sequence galaxies at different locations in the cluster could be a genuine property of the red galaxy population of the cluster, but it could alternatively be caused by the low sensitivity of broad-band colours to small age variation for old stellar populations. Extending the spatial coverage of the cluster is needed however to investigate firmly the differences between galaxy sub-populations of the red sequence.

Figure 10 shows the relationship between the luminosity-weighted ages and metallicities for the galaxies in our sample, separated by morphological type shown in the lower left panel, equivalent width of Hα emission line shown in the lower right panel, and integrated stellar mass shown in the upper panel. Cluster galaxies divide clearly into multiple populations by metallicity and age. The first population is the classic old red sequence galaxies, with ages older than 10-13 Gyr, with predominantly early-type morphologies, and mean metallicities covering a wide range from $\sim$ 10 per cent solar to slightly super-solar. The second group of cluster galaxies, dominated by red sequence lenticular galaxies, covers a similar metallicity range to the first group, but is younger with luminosity-weighted ages ranging between 5 and 10 Gyr. The third group of cluster members contains the younger galaxies populating the blue cloud in the colour-magnitude diagrams, with luminosity-weighted metallicities extending to lower values than those typical for galaxies in the first two groups. Although galaxy luminosity-weighted metallicity is correlated with galaxy mass, it is uncorrelated with luminosity-weighted age for the three populations. Rokas et al. (2008) have used narrow-band colours combined with principal component analysis (Rakos & Schombert 2005) to estimate the luminosity-weighted stellar metallicities and ages for galaxies in a sample of nearby galaxy clusters. They have found cluster early-type galaxies to be divided into two distinct populations, an old galaxy population dominated by primordial stellar populations and a second younger galaxy population, well separated by a gap in age of about 2 Gyr from the oldest galaxies, in agreement with our findings. The third population of cluster galaxies we have identified here is not detected in their analysis, as their technique fails to determine the luminosity-weighted properties for stellar populations dominated by stars younger than $\sim$ 3 Gyr. In addition, galaxies with ongoing star formation or those suspected to have large fractions of young stars identified by their colours and/or strong emission lines were not included in their analysis (see also Rokas et al. 2007). In their sample of nearby galaxy clusters, the populations of bright blue galaxies and faint starburst galaxies are not as populated as in the case of Abell 1367 (see Odell et al. 2002; Rokas et al. 1996).

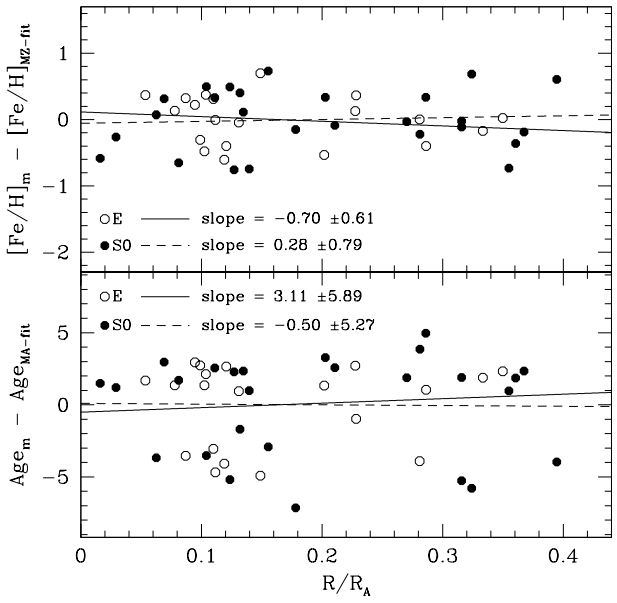

Figure 9. Residuals from the stellar mass-metallicity relation as a function of the normalised projected radius for red sequence ellipticals and S0s respectively.

4 DISCUSSION

A number of studies have analysed absorption line-strength indices of cluster galaxies, and claimed the detection of variation of galaxy properties as a function of cluster-centric radius. Guzmán et al. (1992) reported a positive offset of the zero-point of the relationship between Mg_2 index and galaxy velocity dispersion for massive elliptical galaxies between the core and the outskirts of the Coma cluster. At a fixed velocity dispersion, the Mg_2 line strength is weaker at larger cluster-centric radius. Carter et al. (2002) have used a sample of Coma cluster galaxies extending out to the virial radius, without morphological or colour selection and distributed over a luminosity range similar to galaxies in our sample, to report a significant radial decrease in the Mg_2 index, and an increase of the Hβ index. Carter et al. have attributed the observed radial trends to change in metal abundance at fixed stellar mass between the core and the outskirts of the cluster.

Smith et al. (2008), in a study of 75 red-sequence dwarf galaxies in the Coma cluster, find that the variations in line strength indices are driven by variations in age and in iron abundance, with α-element abundances being independent of radius. Dwarf galaxies in the outer regions of the Coma cluster are on average younger and more iron-enriched than those in the core, at a given luminosity. These results must be treated with caution however, as both of the Coma studies discussed above observed the same, possibly atypical, outer region of the cluster to the southern-west of the core.

Using a sample of ~ 3000 red sequence galaxies dominated by L_* galaxies in ~ 90 nearby clusters, Smith et al. (2006) found strong evidence for stronger Balmer lines and weaker light-element features, at fixed mass, but no radial dependence for iron-dominated indices over a range from the cluster centre to the virial radius. The radial gradients detected for the synthetic cluster formed by stacking galaxies in all clusters in their sample, are significantly shallower than those found for the Coma cluster, with different relative patterns for different spectral indices. Smith et al. (2006) have argued that the observed cluster-centric radial gradients are better explained by a change in the mean age of the dominant stellar populations rather than in metallicity between galaxies in the cores and the outskirts of clusters. Red sequence galaxies at the virial radius have on average younger ages than galaxies of the same velocity dispersion situated near the cluster centres. More recently, Rokas et al. (2007) estimated the cluster-centric radial metallicity gradients for a sample of passive, red galaxies in Abell 1185 cluster. They have found a significant cluster-centric metallicity gradient, with mean metallicities decreasing by ~ 0.2 dex within 40 per cent of the Abell radius of the cluster.

Our analysis shows that the average luminosity-weighted properties of Abell 1367 red sequence galaxies do not show a significant change, at fixed stellar mass, with the location within the cluster over a radial distance ranging from the cluster centre to a radius of approximately half the cluster Abell radius. The complex structure and dynamics of Abell 1367 could lead however to concerns about the extent to which the region covered by our survey is representative of the entire galaxy population of the cluster. In contrast with Smith et al. (2006), the red sequence ellipticals in the core of Abell 1367 appear to be of similar average luminosity-weighted ages than those in the outer regions of the cluster. To account for the observed gradients in star formation rate measured for the CNOC cluster sample, Balogh et al. (2000) have proposed a model in which star-forming galaxies fall into rich clusters and their star formation is gradually quenched by ram pressure and tidal stripping, removing their gas over a few Gyr. This mechanism would be expected to lead to a radial age gradient. In the semi-analytical models of De Lucia et al. (2006), the mean luminosity-weighted age of bulge-dominated galaxies falls from ~ 12 Gyr at the cluster centres to ~ 10.5 Gyr at the virial radius. Some of this effect is due to mass segregation however, as more massive galaxies are preferentially located at the core of the cluster. The restricted range of cluster-centric radial distance covered by our survey, i.e., out to approximately 40 per cent of the virial radius of the cluster, combined with the low sensitivity of broad-band colours to age variation for old stellar populations, projection effects, and the size of the sample means we cannot rule out the presence of a radial age gradient. A comprehensive answer to these concerns should result from an extension of our survey out to the cluster infall region to test if galaxies in other parts of Abell 1367 display similar radial trends.

5 SUMMARY

Using deep optical/near-IR broad-band and narrow-band imaging data, we investigate the stellar population properties for a sample of Abell 1367 galaxies with spectroscopically determined memberships and visual morphological classifications. Our survey samples galaxies with integrated stellar masses ranging from a few 10^8 $M_\odot$ up to a few 10^{11} $M_\odot$. We compare the optical/infrared colours of galax-

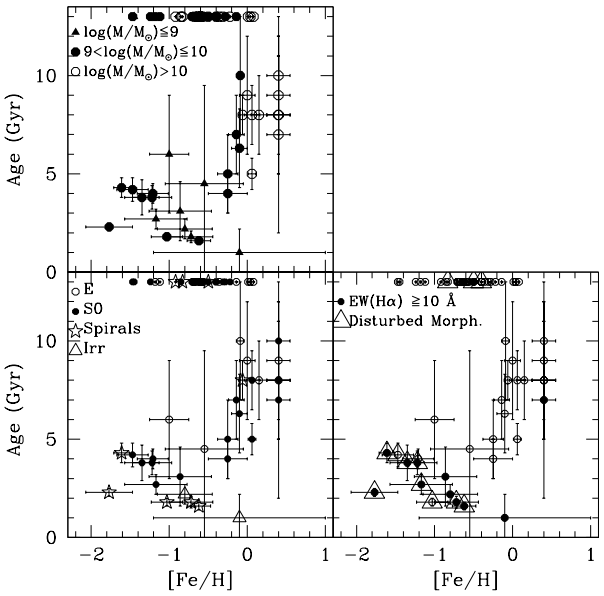

Figure 10. The relationship between the luminosity-weighted stellar metallicity and age for our sample with galaxies separated by morphological type (lower left panel), Hα emission line equivalent width and the presence of signs of morphological disturbance (lower right panel), and stellar mass (upper panel).

ies in our sample with the predictions of simple stellar population models, spanning a range in metallicity and age, to determine the luminosity-weighted parameters of their stellar contents. The colours of galaxies morphologically classified as ellipticals are well described by a sequence of varying metallicity for the stellar population at a constant old age. In contrast, lenticulars along the red sequence show a large spread in their optical/near-IR colours, indicating a spread in the ages and the metallicities of their dominant stellar components.

The stellar population parameters of the cluster galaxies show systematic trends as a function of galaxy stellar mass. We find that the luminosity-weighted properties of galaxy stellar contents correlate with stellar mass in the sense that less massive galaxies are dominated by stellar populations of younger ages and lower stellar metallicities than their massive counterparts. There is however a segregation in the stellar metallicity between quiescent and star forming galaxies. Most of the galaxies which show signs morphological disturbance and have ongoing star formation activity, lie systematically below the stellar mass-metallicity relation defined by galaxies populating the red sequence. The low luminosity-weigthed stellar metallicities of disturbed galaxies could be attributed to tidally-driven gas inflows from the galaxy outskirts which dilute the star-forming gas, leading to less chemically evolved young stars.

We have investigated the cluster-centric radial dependence of the properties of the stellar contents of galaxies. After allowing for the mass dependence of the stellar population properties, we find that the luminosity-weighted properties are not correlated to the cluster-centric radius for galaxies in both the red sequence and the blue cloud, over the radial distance covered by the sample galaxies, i.e., from the cluster centre to approximately half the cluster Abell radius.

The cluster red sequence galaxies are found to be divided into two distinct populations. The first is a subpopulation of elliptical galaxies with uniformly old stellar populations with average ages similar to the age of the Universe. The second sub-population is comprised of red sequence lenticulars with younger ages, for which an age-mass relation is present. None of these two galaxy sub-populations of the red sequence show neither metallicity nor age cluster-centric gradients, over the radial distance covered by the survey. The third cluster subpopulation is that of galaxies where star formation is still ongoing and which are morphologically disturbed.

REFERENCES

Balogh M. L., Navarro J. F., Morris S. L., 2000, ApJ, 540, 113
Barnes J. E., & Hernquist L., 1996, ApJ, 471, 115
Barnes, J. E. 2002, MNRAS, 333, 481
Bell E. F., de Jong R. S., 2001, ApJ, 550, 212
Boselli A., Gavazzi G., Combes F., Lequeux J., Casoli F., 1994, A&A, 285, 69
Boselli A., Gavazzi G., 2006, PASP, 118, 517
Bressan A., Chiosi C., Fagotto F., 1994, ApJS, 94, 63
Burstein D., Faber, S. M., Gaskell C. M., Krumm N., 1984, ApJ, 287, 586
Buta R., 1996, AJ, 111, 591
Butcher H., Oemler A. Jr., 1984, ApJ, 285, 426
Carter D., Mobasher B., Bridges T. J., Poggianti B. M., Komiyama Y., Kashikawa N., Doi M., Iye M., Okamura S., Sekiguchi M., Shimasaku K., Yaki M., Yasuda N. 2002, ApJ, 567, 772
Cortese L., Gavazzi G., Boselli A., Iglesias-Paramo J., Carrasco L., 2004, A&A, 425, 429
De Lucia G., Springel V., White S. D. M., Croton D., Kauffman G., 2006, MNRAS, 366, 499
de Vaucouleurs A., Longo G. 1988, Catalogue of Visual and Infrared Photometry of Galaxies from 0.5 micrometer to 10 micrometer (1961–1985). Univ. of Texas, Austin
Dickey J. M., Gavazzi G., 1991, ApJ, 373, 347
Donnelly R. H., Markevitch M., Forman W., Jones C., David L. P., Churazov E., Gilfanov M., 1998, ApJ, 500, 138
Driver S. P., Popescu C. C., Tuffs R. J., Liske J., Graham A. W., Allen P. D., de Propris R., 2007, MNRAS, 379, 1022
Dressler A., 1980, ApJ, 236, 772
Dressler A., et al., 1997, ApJ, 490, 577
Faber, S. M. 1973, ApJ, 179, 731
Gallazzi A., Charlot S., Brinchmann J., White S. D. M., Tremonti C. A., 2005, MNRAS, 362, 41
Gao L., White S. D. M., Jenkins A., Stoehr F., Springel V., 2004, MNRAS, 355, 819
Gavazzi G., Boselli A., Mayer L., Iglesias-Paramo J., Vílchez J. M., Carrasco L., 2001, ApJ, 563L, 23G
Gavazzi G., Cortese L., Boselli A., Iglesias-Paramo J., Vílchez J. M., Carrasco L., 2003, ApJ, 597, 210
Gavazzi G., Zaccardo A., Sanvito G., Boselli A., Bonfanti, C. 2004, A&A, 417, 499

Grebenev S. A., Forman W., Jones C., Murray S., 1995, ApJ, 445, 607
Godwin J. G., Peach J. V. 1982, MNRAS, 200, 733
Gratton R. G., Bonifacio P., Bragaglia A. et al., 2001, A&A, 369, 87
Guenther D. B., 1994, ApJ, 422, 400
Guzmán R., Lucey J. R., Carter D., Terlevich R. J., 1992, MNRAS, 257, 187
Hempel M., Kissler-Patig M., 2004, A&A, 428, 459
James P. A., Salaris M., Davies J. I., Phillipps S., Cassisi S., 2006, MNRAS, 367, 339
Katz N., White S. W. D., 1993, ApJ, 412, 455
Kennicutt R. C. 1998, ARA&A, 36, 189
Kewley L. J., Geller M. J., Barton E. J. 2006, AJ, 131, 2004
Kewley L. J., Rupke D., Jabran Z. H., Geller M. J., Barton E. J., 2010, ApJ, 721L, 48
Korn A. J., Grundahl F., Richard O., Barklem P. S., Mashonkina L., Collet R., Piskunov N., Gustafsson B. 2006, Nat, 442, 657
Lane K. P., Gray M. E., Aragón-Salamanca A., Wolf C., Meisenheimer K., 2007, MNRAS, 378, 716
Lee H., Worthey G., Trager S. C., Faber S. M., 2007, ApJ, 664, 215
Lewis I., et al., 2002, MNRAS, 334, 673
Kroupa P., 2001, MNRAS, 322, 231
MacArthur L. A., Courteau S., Bell E., Holtzman J., 2004, ApJS, 152, 175
Mihos, J. C., & Hernquist, L. 1996, ApJ, 464, 641
Michel-Dansac L., Lambas D. G., Alonso M. S., Tissera P., 2008, MNRAS, 386, 82
Montuori M., Di Matteo P., Lehnert M. D., Combes F., Semelin B., 2010, A&A, submitted (arXiv:1003.1374)
Moss C., Whittle M., Pesce J. E., 1998, MNRAS, 300, 205
Moss C., Whittle M., 2000, MNRAS, 317, 667
Moss C., Whittle M., 2005, MNRAS, 357, 1337
Moss C., 2006, MNRAS, 373, 167
Nelan J. E., Smith R. J., Hudson M. J., Wegner G. A., Lucey J. R., Moore S. A. W., Quinney S. J., Suntzeff N. B., 2005, ApJ, 632, 137
Odell A. P., Schombert J., Rakos K., 2002, AJ, 124, 3061
Peeples M. S., Pogge R. W., Stanek K. Z., 2009, ApJ, 695, 259
Peletier R. F., Valentijn E. A., Jameson R. F., 1990, A&A, 233, 62
Peletier R. F., Balcells M., 1996, AJ, 111, 2238
Pietrinferni A., Cassisi S., Salaris M., Castelli F., 2004, ApJ, 612, 168
Poggianti B., 1997, A&AS, 122, 399
Puzia T. H., Zepf S. E., Kissler-Patig M., Hilker M., Minniti D., Goudfrooij P., 2002, A&A, 391, 453
Rakos K., Maindl T. I., Schombert J., 1996, ApJ, 466, 122
Rakos K., Schombert J., 2005, AJ, 130, 1002
Rakos, K., Schombert, J., Odell, A., 2007, ApJ, 658, 929
Rakos, K., Schombert, J., Odell, A., 2008, ApJ, 677, 1019
Rose J. A., 1985, AJ, 90, 1927
Rose J. A., Bower R. G., Caldwell N., Ellis R. S., Sharples R. M., Teague P., 1994, AJ, 108, 2054
Rupke D. S. N., Veilleux S., Baker A. J., 2008, ApJ, 674, 172
Rupke D. S. N., Kewley L. S., BArnes J. E., 2010, ApJ Letters, 710, 156
Sánchez-Blázquez P., Gorgas J., Cardiel N., González J. J., 2006, A&A, 457, 809
Sakai S., Kennicutt R. C., van der Hulst J. M., Moss C., 2002, ApJ, 578, 842
Schlegel D. J., Finkbeiner D. P., Davis M., 1998, ApJ, 500, 525
Schiavon R. P., 2007, ApJS, 171, 146
Schombert J., Rakos K., 2009a, AJ, 137, 528
Schombert J., Rakos K., 2009b, ApJ, 699, 1530
Smail I., Kuntschner H., Kodama T., Smith G. P., Packham C., Fruchter A. S., Hook R. N., 2001, MNRAS, 323, 839
Smith R. J., Hudson M. J., Lucey J. R., Nelan J. E., Wegner G. A., 2006, MNRAS, 369, 1419
Smith R. J., Marzke, R. O., Hornschemeier A. E., Bridges, T. J., Hudson M. J., Miller N. A., Lucey J. R., Vázquez G. A., Carter, D. 2008, MNRAS, 386, 96
Struble M. F., Rood H. J., 1999, ApJS, 125, 35
Sun M., Murray S. S. 2002, ApJ, 576, 708
Taylor V. A., Jansen R. A., Windhorst R. A., Odewahn S. C., Hibbard J. E., 2005, ApJ, 630, 784
Terlevich, A. I., Caldwell, N., Bower, R. G. 2001, MNRAS, 326, 1547
Terlevich A. I., Forbes D. A. 2002, MNRAS, 330, 547
Thomas D., Maraston C., Bender R. 2003, MNRAS, 339, 897
Thomas D., Maraston C., Bender R., Mendes de Oliveira C., 2005, ApJ, 621, 673
Vazdekis A., 1999, ApJ, 513, 224
West M. J., Villumsen J. V., Dekel A., 1991, ApJ, 369, 287
Worthey G., 1994, ApJS, 95, 107
Worthey G., Ottoviani D. L., 1997, ApJS, 111, 377
Zaritsky D., Kennicutt R. C., Jr., & Huchra J. P. 1994, ApJ, 420, 87

This paper has been typeset from a TEX/ LATEX file prepared by the author.